Hindawi
International Journal of Aerospace Engineering
Volume 2019, Article ID 5620124, 10 pages
https://doi.org/10.1155/2019/5620124

Research Article

Study on Initial Disturbance of Airborne Missile's Horizontal Backward Derailment under Continuous Gust

Xiao Pan, Yi Jiang, Xinlin Wei, and Mingjun Li

School of Aerospace Engineering, Beijing Institute of Technology, Beijing 100081, China

Correspondence should be addressed to Yi Jiang; jy2818@163.com

Received 21 January 2019; Accepted 10 October 2019; Published 12 November 2019

Academic Editor: Linda L. Vahala

This paper studies the effect of continuous gusts on the initial disturbance of the airborne missile's horizontal backward derailment on large transport aircraft. The longitudinal fluctuation of the airborne launching platform under continuous gust was obtained with different calculation methods, and the finite element model of the derailing process was established then verified by experiments. Finally, combined with the longitudinal fluctuation of the launching platform and the finite element model of the missile and launching platform, the influence of platform fluctuation on separation time, missile speed, pitch angle, and descending distance while derailing was studied and analyzed. It is found that the longitudinal fluctuation of the launching platform is similar to that of the gust but lags behind, and the missiles under the fluctuating platform have longer separation time, lower derailing speed, and greater derailing pitch angle and descending distance.

1. Introduction

The airborne missile's horizontal backward launch is a way to launch the missile using a large transport aircraft. After the missile acquires a certain ejection speed through the ejection device, it glides backwards on the horizontal guide rail on the launching platform until derailed and completely separated, then ignites at a distance from the aircraft. The process can be shown in Figure 1. Predicting the launching effect of this method is closely related to the fluctuation response of the launching platform under the gust load, especially the initial disturbance of the missile at the time of derailing; thus, studying the effect of continuous gusts on the initial disturbance of the airborne missile's horizontal backward derailment on large transport aircraft is necessary.

Skelton presented an analytical technique for the design of gust alleviation controls for the boost-phase flight of missiles [1]. In Surace and Pandolfi's study [2], the finite element method incorporating an atmospheric turbulence model and a structural model is used to analyze the vibration characteristics of missiles and is applied to random vibrations excited by gust loads. Liao established launch dynamics and kinematics models and analyzed some influencing factors, including pneumatic force and stochastic wind disturbance [3]. In this paper, the atmospheric disturbance is the main influencing factor of the longitudinal fluctuation on an airborne launching platform. In order to obtain the aircraft motion equations under gust disturbance, the Von Karman model was chosen as the continuous gust model for calculating atmospheric disturbance response, and a longitudinal fluctuation theory model of the launching platform was built to get the theoretical calculation results. At the same time, the flow field simulating model of the aircraft under unsteady wind field is established, and the simulation results were used to compare with the theoretical results above. The theoretical calculation results are analyzed to prove the correctness of the theoretical model. In the research of the initial disturbance of the missile derailment, a finite element model was established, and the initial disturbance of the missile was calculated and verified by the ground test. Finally, the derailing process under the vertical fluctuation of the platform is calculated, and the influence of platform fluctuation on the initial disturbance of the missile derailment is analyzed.

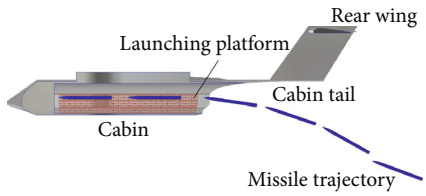

Figure 1: Horizontal backward launch.

2. Longitudinal Fluctuation Model of Launching Platform

2.1. Theoretical Calculation of Launching Platform's Longitudinal Fluctuation Model. The gust includes discrete gust and continuous gust. The discrete gust model is used to represent a single discrete extreme turbulence wind, and the continuous gust model represents a longer turbulent process while considering slight attenuation. In aircraft strength calculation and aircraft control system design, the (1-cosine) discrete gust model is widely used [4]. In the study of gust load mitigation control, Hu [5] used the (1-cosine) discrete gust model as input to calculate the response of various components of an elastic aircraft. Gao [6] verified the control effect of the aircraft's mitigation algorithm under the gust load by means of the (1-cosine) discrete gust model. Also, the full-fluctuation length (1-cosine) discrete gust model is specified in the airworthiness standard for transport aircraft [7].

Continuous gusts need to be described by the stochastic theory. Currently, the turbulence models widely used to calculate the power spectral density of the gust velocity are the Dryden model and the Von Karman model. The autopower spectral density function of gust speed under the Dryden model is

$$\Phi(\Omega) = \frac{\sigma^2 L}{\pi} \frac{1 + (3L\Omega)^2}{\left[1 + (L\Omega)^2\right]^2}, \tag{1}$$

where Φ is the power spectral density, σ is the root mean square value of the gust speed, and L is the turbulence size, while the autopower spectral density function of gust speed under the Von Karman model is

$$\Phi(\Omega) = \frac{\sigma^2 L}{\pi} \frac{1 + (8/3)(1.339L\Omega)^2}{\left[1 + (1.339L\Omega)^2\right]^{11/6}}. \tag{2}$$

The Von Karman model is a turbulence model based on theoretical and experimental measurements while the Dryden model is a simplification of the former [8]. The two models are usually similar in the low band and differ at high frequencies. In the study of flight quality related to aircraft structural vibration, aircraft structural fatigue, and other issues, the aircraft structural modal frequency is usually in the high frequency range and the turbulence in this range may stimulate the structural vibration of the aircraft; thus, the Von Karman model can usually produce a good calculation result [9]. Also, the Von Karman model is adopted for the continuous gust model in the airworthiness standard of transport aircraft [7].

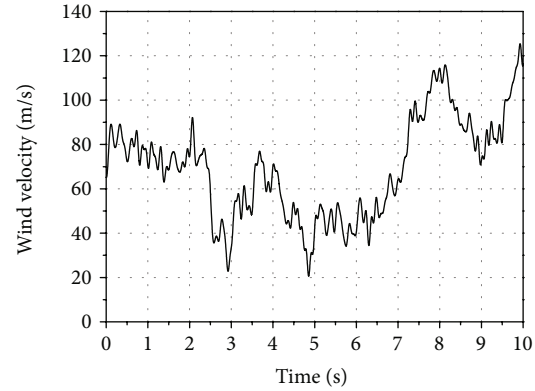

Figure 2: Continuous gust time domain model.

Chen [10] uses the difference equation to solve for the time domain model of the Dryden filter, obtains the signals of the longitudinal atmospheric turbulence components, and solves for the response of the aircraft under continuous atmospheric turbulence; many scholars [5, 6, 11] have calculated the gust response of the elastic aircraft based on the Von Karman continuous gust model in the study of the aircraft gust response simulation method and load mitigation technology.

In summary, the Von Karman model is used as the continuous gust model in the calculation of atmospheric disturbance response. According to the gust spectral density function and the discrete formula of the simulated stationary Gaussian stochastic process, continuous atmospheric gust disturbance can be generated by MATLAB. Set the discrete frequency upper limit value $f_u = 10$, the discrete frequency lower limit value $f_i = 0$, the turbulence scale $L = 760$, the aircraft flow speed $V = 80$, and the aircraft flight altitude $h = 8000$. The generated continuous gust time domain model is shown in Figure 2.

Assuming that the disturbance of the gust to the aircraft is W, the aircraft's centroid equation of motion can be obtained as follows:

$$\begin{cases} \dot{V}_\chi = \dfrac{X}{m} - \dot{W} - g\sin\theta - \left(q_B V_z - r_B V_y\right), \\ \dot{V}_y = \dfrac{Y}{m} - \dot{W} + g\sin\phi\cos\theta - \left(r_B V_\chi - p_B V_z\right), \\ \dot{V}_z = \dfrac{Z}{m} - \dot{W} + g\cos\phi\cos\theta - \left(p_B V_y - q_B V_\chi\right). \end{cases} \tag{3}$$

When there is a gust, the aircraft's rotational equations above do not change, but the aerodynamic and aerodynamic moments of the aircraft are affected, so the relevant aerodynamic parameters need to be corrected. Those aerodynamic parameters include the derivative of the attack angle $\dot{\alpha}$ and side slip angle $\dot{\beta}$ and rotating angular velocities p, q, and r. Based on the aircraft's centroid equation of motion with the disturbance gust parameter added, $\dot{V}_x$, $\dot{V}_y$, and $\dot{V}_z$ can be calculated and then $\dot{\alpha}$ and $\dot{\beta}$ can be obtained. Based on the

Table 1: Calculation parameters.

Parameter	Value
Flight altitude (m)	8000
Flight speed (m/s)	80
Air density (kg/m^3)	0.54
Aircraft weight (kg)	271632
Pitch moment of inertia (kg/m^2)	2.6×10^{13}

four-point model and considering the gradient effect of the gust, the angular velocity of the aircraft after the disturbance of the air can be obtained, which is associated with p, q, and r. Since this paper only considers the fluctuation response of the aircraft after gust disturbance in the longitudinal plane, the equation of motion of the aircraft under gust disturbance can be simplified as follows:

$$\begin{cases} \dot{q}_B = \dfrac{M}{I_y}, \\ \dot{V}_x = \dfrac{X}{m} - \dot{W}_{xB} - g\sin\theta - q_B(V_z + W_{zB}), \\ \dot{V}_z = \dfrac{Z}{m} - \dot{W}_{zB} + g\cos\theta - q_B(V_x + W_{xB}). \end{cases} \tag{4}$$

Let the disturbance gust in the geodetic coordinate system be W_{xg}, then

$$\begin{cases} \dot{W}_{xB} = \dot{W}_{xg}\cos\theta - W_{xg}\sin\theta, \\ W_{zB} = W_{xg}\sin\theta, \\ \dot{W}_{zB} = \dot{W}_{xg}\sin\theta + W_{xg}\cos\theta, \\ W_{xB} = \dot{W}_{xg}\cos\theta, \\ \alpha = \arctan\left(\dfrac{V_z + W_{zB}}{V_x + W_{xB}}\right), \\ Z = -C_{c\alpha}\rho\dfrac{S}{2}\left((V_x + W_{xB})^2 + (V_z + W_{zB})^2\right), \\ M = (Z + Z_0)\bar{c}. \end{cases} \tag{5}$$

The initial state of the aircraft can be expressed as

$$\begin{cases} X_0 = mg\sin\theta_0, \\ Z_0 = mg\cos\theta_0, \\ M_0 = 0. \end{cases} \tag{6}$$

Using the continuous gust model as the atmospheric disturbance input and combining with the fluctuation response of the aircraft in the longitudinal plane, the solution is solved by MATLAB/Simulink to obtain the theoretical longitudinal fluctuation response of the platform under the continuous gust. The calculation parameters are as shown in Table 1.

Figures 3, 4, and 5 are the curves of the displacement, velocity, and acceleration of the aircraft's longitudinal fluctuation under atmospheric disturbance. According to the figures, the aircraft is in the downward movement during this 10 s time period, and the maximum descending distance is 17.30 m. The speed increases in the negative direction, reaching the maximum value 4.56 m/s at 7.7 s and then decreasing to the initial state. The longitudinal acceleration of the aircraft fluctuates throughout the calculation, reaching the negative maximum value 3.08 m/s^2 at 3.9 s and the positive maximum value 4.01 m/s^2 at 8.9 s.

In summary, during the flight of 10 s, the aircraft experienced a descending process of first lowering the head

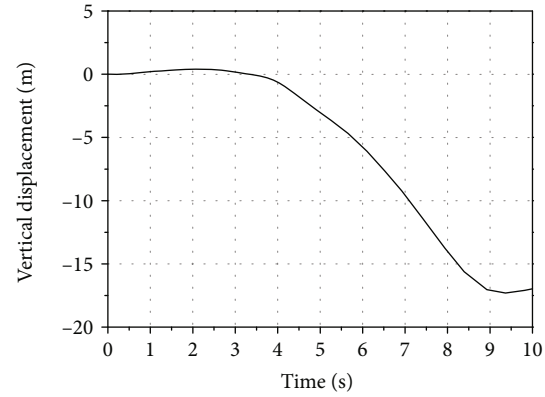

Figure 3: Aircraft longitudinal displacement.

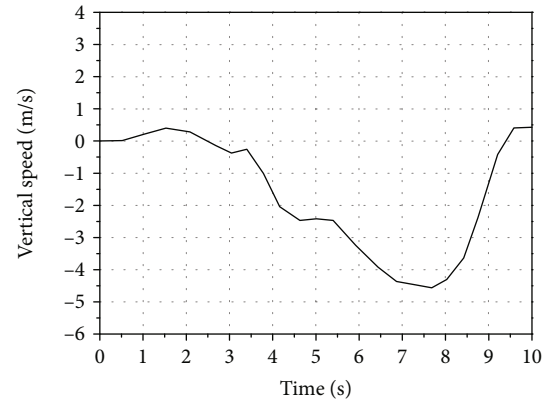

Figure 4: Aircraft longitudinal speed.

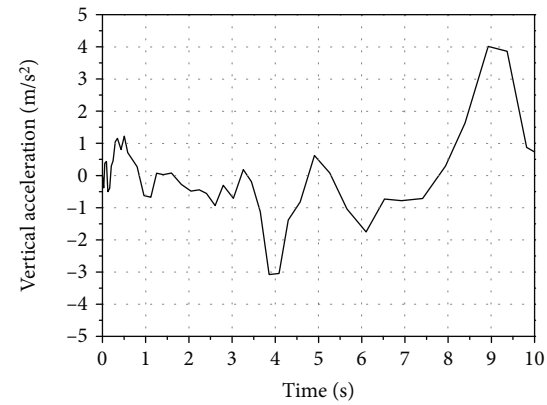

Figure 5: Aircraft longitudinal acceleration.

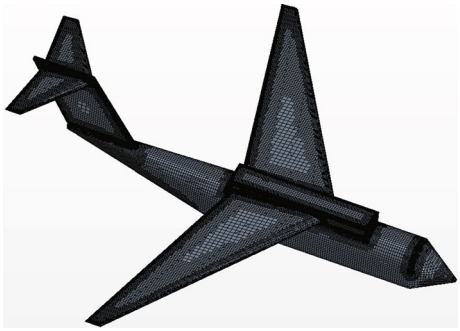

Figure 6: Mesh on the aircraft surface.

and accelerating, then raising the head and slowing down, which is consistent with the movement of the aircraft during the cruise.

2.2. Simulation of Launching Platform's Longitudinal Fluctuation Model. In order to verify the correctness of the longitudinal fluctuation model of the platform, it is necessary to establish a flow field CFD calculation model for simulation and compare the fluctuation response of the airborne launch platform under the gust load with Section 2.1. Assuming that

(1) the aircraft can be considered rigid

(2) the aircraft is under only the effect of longitudinal gust

(3) the speed of the gust is generated in Section 2.1

In this section, the space-time second-order precision finite volume method is used to discretize the three-dimensional, compressible and viscous NS equations. The standard turbulence model is used to describe the turbulence effect of the flow field, and the coupled solution method is used to solve the discrete algebraic equations to obtain the numerical solution of the flow field change. We use the nested mesh technology [12, 13] to study the coupling of aircraft motion and flow field change, then integrate the pressure distribution of the aircraft to solve the lift of the aircraft and obtain the single-degree-of-freedom motion equation and longitudinal motion of the aircraft. The mesh is divided into two regions: one is the overall background mesh and the other is the nested mesh containing the aircraft. The background mesh is refined in the area where the nested mesh may pass and on the surface of the aircraft, especially in areas with sharp geometric changes such as wing edges, as shown in Figures 6 and 7. The calculation parameters in this section are consistent with Section 2.1, where the atmospheric parameters are selected according to the standard atmospheric table as shown in Table 1, and the wind speed input is the continuous gust time domain model generated in Section 2.1.

2.3. Comparison of Theoretical and Simulation Results. In order to verify the correctness of the model, the CFD calculation results within 30 s are compared with the MATLAB/Simulink solution results. The longitudinal velocity variation of the aircraft is shown in Figure 8.

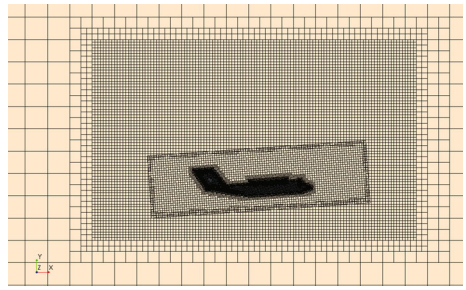

Figure 7: Mesh on aircraft symmetry plane.

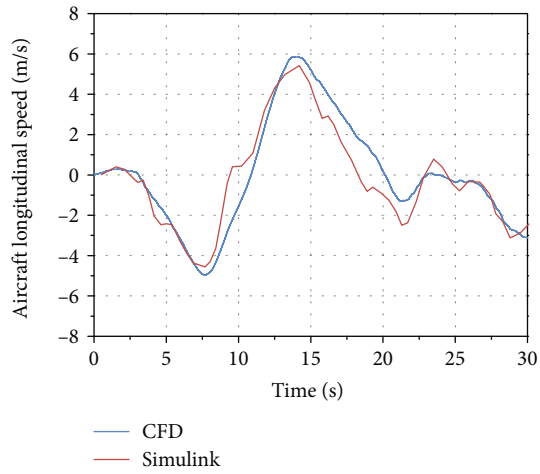

Figure 8: Aircraft longitudinal speed comparison rail is fixed in the adapters [19]. The main structure is shown in Figures 9 and 10.

Figure 8 shows that the MATLAB/Simulink results are consistent with the CFD calculation. At $t = 7.7$ s, the longitudinal velocity of the aircraft reaches the minimum value in both calculations. The minimum value of the MATLAB/-Simulink calculation is -4.57 m/s, and the minimum value of the CFD calculation is -4.96 m/s. The relative error is 7.86%. At 14.2 s, the maximum value of the MATLAB/Simulink calculation is 5.42 m/s, the maximum value of the CFD calculation is 5.79 m/s, and the relative error is 6.39%. The main reasons for the error are as follows: (1) When the equation of motion is used to solve the attitude of the aircraft in the event of gusting, the lift of the aircraft in the equation is based on the empirical formula and the lift coefficient and focal position of the aircraft are uncertain. (2) When the CFD calculation method is used to solve the attitude of the aircraft in the gust disturbance, the calculation result is related to the quality of the flow field mesh and the calculation method of the flow field, and only a relatively close realistic result can be obtained [14].

Comparing the longitudinal displacement, velocity, and acceleration of the launching platform's longitudinal fluctuation model with the gust input, it can be found that the longitudinal fluctuation of the launching platform is similar to that of the gust but lags behind. With the fluctuation of the gust, the aircraft presents a state of ups and downs. When the gust speed increases, the aircraft's lift, the forward acceleration, and the longitudinal speed increase, and the aircraft

is ascending. When the gust speed decreases, the aircraft's lift, the forward acceleration, and the longitudinal speed increase, and the aircraft is descending. This indicates that the gust load has a significant impact on the longitudinal fluctuation of the aircraft, which will have a greater impact on the safety of the missile launch. Therefore, the longitudinal fluctuation response of the launch platform must be considered in the airborne missile's horizontal backward launching process.

3. Analysis of Missile Horizontal Derailment Process

Different designs of the launching system have been made for different requirements for the launch mode of airborne missiles [15–17], and their effects are studied by scholars [18]. The launching platform in this article consists of two carrier racks, each with 9 positions and a maximum load of 18 for the entire launching platform. The missile is matched with four guide rails through three sets of adapters (four adapters in each set) and the outer side of the guide.

The ejection force of the missile is provided by the catapult device, which requires the missile to be ejected to an initial speed within a displacement of 2 m [20].

The research in this paper includes the fixed and fluctuating conditions of the launching platform. When the platform is fixed, the bottom surface of the platform is fixed to the carrier, so the boundary condition is set to be fixed. Under the fluctuation condition, the launching platform of the airborne missile is fixed to the carrier and moves with it. Therefore, in the finite element simulation, the longitudinal fluctuation of the platform obtained by Section 2.1 is used as the boundary condition.

3.1. Simulation of Fixed Platform's Derailment Process. This section simulates the derailment process of the missile on the fixed platform and obtains the initial disturbance of the missile such as the speed of the missile, the distance of descent, and the derailing attitude angle. The simulation results are as follows: Figure 11 is the longitudinal displacement of the missile's centroid. While the platform is fixed, the parameter directly reflects the missile's descending distance during the derailment process. It can be seen from the figure that at the time 1.96 s, the first set of adapters leaves the rail and the longitudinal displacement of the missile centroid slightly fluctuates because the pitch angle of the missile becomes smaller when the first set of adapters are completely separated, resulting in a small increase in the centroid displacement. As the adapter gradually separates, the pitch angle of the missile increases and the missile's descending distance increases.

Figure 12 is the speed of the missile's centroid. As can be seen from the figure, the missile is accelerated to obtain an ejection speed of 11.48 m/s before it slips in the guide rails. As three sets of adapters are sequentially derailed, the speed of the missile fluctuates and a large change occurs when the last set of adapters derails. During the entire derailment process, the missile continuously loses its speed under the collision with the guide rails [21].

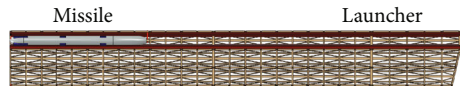

Figure 9: Launching platform and missile.

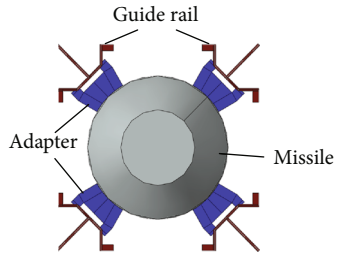

Figure 10: Missile and guide rail assembly diagram.

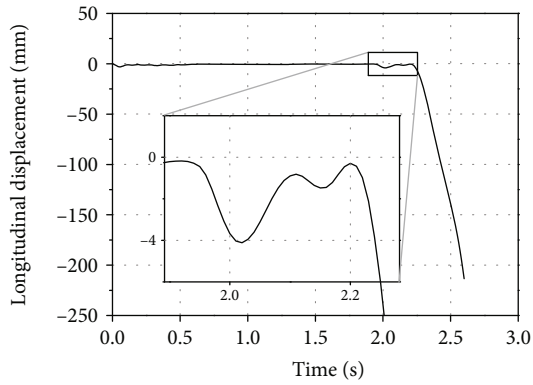

Figure 11: Longitudinal displacement of the center of mass of the missile under the fixed platform.

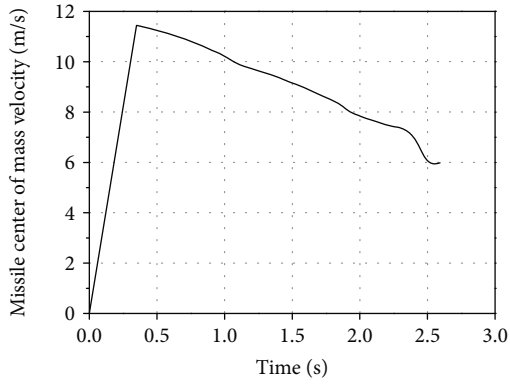

Figure 12: The speed of the missile's centroid under the fixed platform.

Figures 13 and 14 show the pitch angle and angular velocity of the missile during the derailment process, respectively. It can be seen from the figure that the pitching of the missile is relatively stable before the adapter derails; the pitch angle and angular velocity are both close to zero. When the adapter starts to derail, a certain pitch angular velocity is gradually obtained under the action of its own gravity. As the adapter gradually derails, the pitch angular velocity increases continuously and reaches a maximum value of 16.78 deg/s at 2.41 s. The pitch angle of the missile increases from 1.96 s as

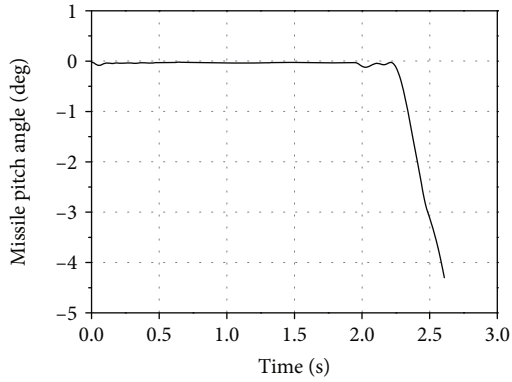

Figure 13: The pitch angle of the missile under a fixed platform.

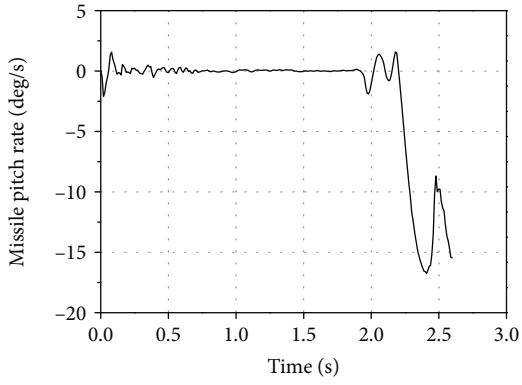

Figure 14: The pitch angular velocity of the missile under a fixed platform.

the first set of adapters leaves the rail and reaches a maximum of 4.26 deg when the third set of adapters is completely separated. The results show that the separation of the adapter is the direct cause of the change of the missile's pitch.

In summary, in the case of the fixed platform's derailment process, the missile attitude change mainly occurs at the time of adapter separation. As the three sets of adapters are separated in sequence, the pitch angle and sinking amount of the missile gradually increase.

3.2. Ground Ejection Test of Fixed Platform's Derailment Process. In order to verify the finite element analysis model of the horizontal backward missile-launching derailment, a single-shot missile-launching device was built to perform the missile's derailment process under a fixed platform. The ground ejection test is used to compare with the derailment-simulating results under a fixed platform. The launching device is shown in Figure 15.

Table 2 gives a comparison of the simulation results of the derailment velocity and the experimental results. It can be seen that the simulations agree well with the experimental results (v_1: ejection speed; v_2: derailment speed).

3.3. Analysis of Initial Disturbance of Horizontal Backward Ejection Derailment. The missile's derailment process is one of the key processes for an airborne missile's horizontal backward launch, which determines whether the initial disturbance of the missile meets launching requirements after derailment.

Figure 15: Ground ejection test site.

Table 2: Missile derailment speed simulation and test results.

Observation object	Test value	Simulation calculated value	Relative error
Time (s)	2.50	2.60	4.00%
v_1 (m/s)	11.51	11.475	-0.22%
v_2 (m/s)	5.86	6.00	2.43%

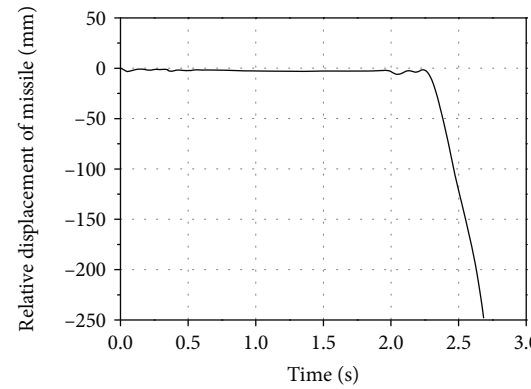

Figure 16: Longitudinal relative displacement of the missile centroid under the fluctuating platform.

While under the gust environment, the derailment process of missiles with large span and long guide rails becomes more complicated [22–24]. The longitudinal fluctuation of the platform obtained in Section 2 can be taken as the input to calculate the finite element simulation result and compare with the calculation result under the fixed platform. Through the calculation of various working conditions, the influence of the ejection velocity and the launch tilt angle on the initial disturbance of the derailment is analyzed and discussed.

Based on the finite element analysis model of missile derailment established in Section 3.1, this section uses the longitudinal fluctuation of the platform as the boundary condition to simulate the missile's derailment process and obtain the initial disturbance such as the speed and descending distance of the missile. The simulation results are as follows.

Figure 16 shows the longitudinal relative displacement of the missile's centroid to the launching system. It can be seen from the figure that at time 1.89 s, the first set of adapters leaves the rail and the longitudinal displacement of the missile centroid slightly fluctuates. It happens because when the adapter is completely separated, the pitch angle falls instantaneously. As the missile glides in the guide rail, the pitch angle and the descending distance of the missile increase. After the third set of adapters is completely separated, the maximum longitudinal relative displacement is 246.48 mm.

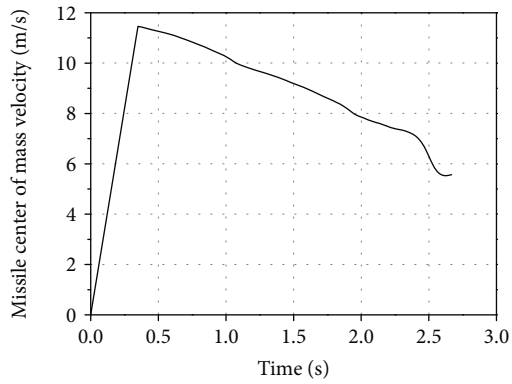

Figure 17: Missile centroid velocity under the fluctuating platform.

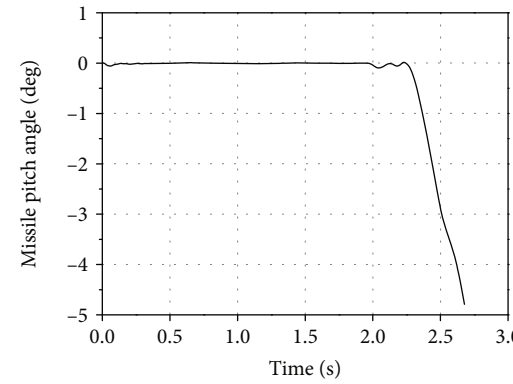

Figure 18: The pitch angle of the missile under the fluctuating platform.

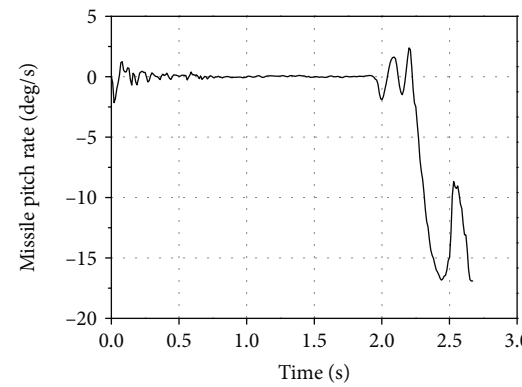

Figure 19: The pitch angular velocity of the missile under the fluctuating platform.

Figure 17 shows the velocity of missile's derailment under platform fluctuations. It can be seen from the figure that the missile first obtains a higher ejection speed through the ejection acceleration section as it does in the fixed platform, reaching 11.48 m/s. Then, it began to glide in the guide rail. As the three sets of adapters were sequentially derailed, the speed of the missile began to fluctuate. When the last set of adapters derailed, a large change occurred, and the final derailment speed was 5.58 m/s. As the adapter deviates from the rail and the platform fluctuates, the missile begins to pitch and sink, and the longitudinal velocity begins to increase, reaching 0.99 m/s when it finally derailed. During the entire derailment process, the missile continuously loses energy under the collision with the guide rail, especially at the moment when the adapter derails where the speed of the missile changes greatly.

Figures 18 and 19 show the pitch angle and angular velocity of the missile during the derailment process, respectively. It can be seen from the figure that in the fluctuating environment, the pitching motion of the missile derailment is similar to that of the platform in the fixed environment. The missile is stable before the adapter derails, and the pitch angle and angular velocity are both close to zero. When the adapter starts to derail, under the action of the torque generated by its own gravity, a certain pitch angular velocity is gradually obtained, and as the adapter gradually derails, the pitch angular velocity increases continuously and reaches the first trough 16.84 deg/s in 2.44 s. At this point, the second set of adapters has been separated, and the third set of adapters is beginning to derail. The pitch angle of the missile increases from 1.98 s when the first set of adapters separates and reaches a maximum of 4.78 deg when the third set of adapters is completely separated. This shows that in the case of fluctuations in the launch platform, the separation of the adapter is still the direct cause of change in the pitch angle of the missile.

In summary, in the case of platform fluctuations, the longitudinal movement of the missile changes. In this chapter, the focus is on the initial disturbance of the missile relative to the launching platform. Therefore, in the subsequent comparative analysis, the initial disturbance of the derailment relative to the launching platform is analyzed and discussed.

3.4. Comparative Analysis of the Fixed Platform and the Fluctuation Platform. In this section, the results of the fixed and fluctuating launching platforms are compared and the influence of the longitudinal fluctuation of the platform on the initial disturbance of the missile derailment is analyzed.

According to Figure 20, the speed change of the missile under two conditions is similar from acceleration to derailment. The final derailment speed is 6.00 m/s under the fixed platform, and the final derailment speed is 5.58 m/s under the fluctuating platform. Through comparative analysis, after the same ejection acceleration section, the missile's derailment speed is lower under the fluctuation platform which is 7.00% lower than the fixed platform's derailment speed. This is due to the severe frictional collisions between the missile adapter and the guide rail caused by the platform fluctuation, which result in more loss of kinetic energy.

Figure 21 shows the longitudinal displacement of the missile's centroid relative to the launching system under two conditions. The trend of the two is more consistent, but the displacement value at the time of the derailment is slightly different. Under the fixed platform, the missile's centroid descending distance is 213.47 mm, and the missile's centroid descending distance is 246.48 mm when the platform fluctuates: the amount of missile centroid descent increases by 15.46% compared with that of the fixed platform. This is because the longitudinal relative motion of the launching platform during the missile's derailment is larger, which can increase the missile's descent.

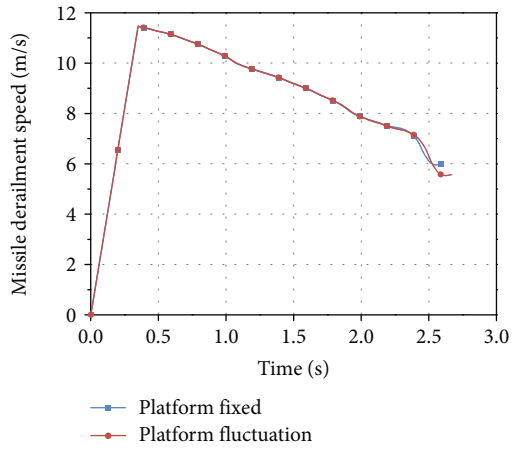

Figure 20: Missile derailment speed under two platforms.

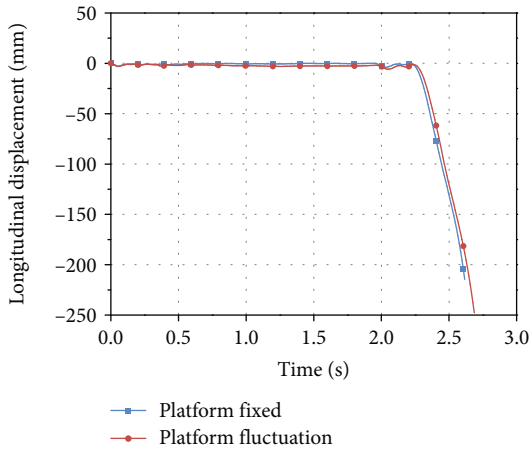

Figure 21: Longitudinal displacement of missiles under two platforms.

Figure 22 shows the curve of the pitch angle during the missile's derailment process under two conditions. It can be seen that the trend of the two is consistent before the second set of adapters derails. The missile's derailment pitch angle is 4.26 deg under the fixed platform, and the missile's derailment pitch angle is 4.78 deg under the fluctuating platform. Under the fluctuating platform, the missile's derailment pitching angle is increased by 12.20% compared with the fixed platform. This is directly related to the longitudinal relative motion of the missile caused by the longitudinal fluctuation of the platform, which intensifies the pitching motion of the missile and increases the pitch angle.

Table 3 shows the attitude comparison of each group of adapters when they are leaving the rail in both working conditions. v_m is the missile's speed, θ_m is the missile's pitch angle, Y is the centroid descending distance, S_{1f} is the situation where the first set of adapters separate at the fixed platform, S_{2v} is the situation where the second set of adapters separate at the fluctuating platform, and so on. According to the data in Table 3, the separation time of the three sets

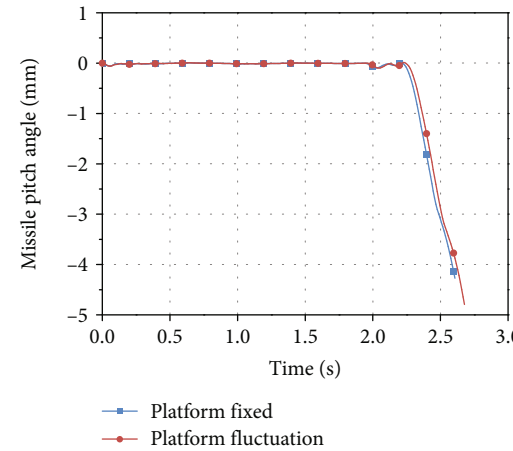

Figure 22: Missile pitch angle under two platforms.

Table 3: Attitude comparison of each group of adapters under derailment under two working conditions.

	Time (s)	v_m (m/s)	θ_m (deg)	Y (mm)
$S1f$	1.96	7.96	0.019	0.85
$S1v$	1.98	7.91	0.020	2.78
$S2f$	2.22	7.48	0.016	0.98
$S2v$	2.25	7.41	0.031	2.93
$S3f$	2.60	6.00	4.261	213.47
$S3v$	2.67	5.58	4.781	246.48

of missiles under the fluctuating platform lags by 0.02 s, 0.03 s and 0.07 s, respectively. The speed of the missiles in each group is reduced by 0.63%, 0.94%, and 7.09%, respectively, which reflects that the missile's derailment speed is affected by the longitudinal fluctuation of the platform. At the same time, the longitudinal fluctuation of the platform also causes a small lag in the separation time of each group of adapters, and the pitch angle and relative descending distance on the derailment time under the fluctuating platform increase by 12.20% and 15.46%, respectively, relative to the fixed platform. It indicates that under the influence of longitudinal fluctuation of the platform, the initial disturbance of the missile's derailment is greatly affected. In the study of the initial disturbance of the airborne missile's horizontal backward derailment, the platform fluctuation cannot be ignored.

4. Conclusion

In this paper, by comparing the MATLAB/Simulink calculation model and CFD calculation model of the longitudinal fluctuation of the airborne platform under the influence of continuous gusts, the longitudinal fluctuation of the airborne launching platform under the gust load is analyzed, using the ground test data to verify the finite element derailment simulation model. Finally, the longitudinal fluctuation of the airborne launching platform under the gust load is combined

with the verified finite element model to research the influence of platform fluctuation on separation time, missile speed, pitch angle, and descending distance while derailment was studied and analyzed. Through the analysis of the results, the following conclusions can be drawn:

(1) The calculation results of MATLAB/Simulink under the Von Kaman model are in good agreement with the airborne platform's longitudinal fluctuations under the influence of continuous gusts in the CFD flow field calculation model, which verifies the correctness of the theoretical model

(2) The gust load has a significant impact on the longitudinal fluctuation of the aircraft. The longitudinal acceleration, velocity, and displacement of the aircraft are similar to those of the gust but lag behind. While the airborne launching platform is in the longitudinal fluctuation when performing the launching task, this will have a greater impact on the missile-launching effect. Therefore, the longitudinal fluctuation response of the launching platform must be considered in the study of the horizontal launching of the airborne missile

(3) The fixed finite element calculation model of the platform is in good agreement with the experimental results. Therefore, the finite element calculation of the dynamic state of the missile's horizontal backward launch orbit is accurate and credible

(4) The platform fluctuation has a great influence on the initial disturbance of the missile. The platform fluctuation causes the missiles to have a longer separation time, lower derailing speed, and greater derailing pitch angle and descending distance. Therefore, in the study of the initial disturbance of the airborne missile's horizontal backward derailment, the platform fluctuations cannot be ignored

Data Availability

The test data used to support the findings of this study are included within the article.

Conflicts of Interest

The authors declared no potential conflicts of interest with respect to the research, authorship, and/or publication of this article.

References

[1] G. Skelton, "Launch booster gust alleviation," in *3rd Annual Meeting*, Boston, MA, USA, November-December 1966.

[2] G. Surace and M. Pandolfi, "Calculation of missile vibrations," in *Associazione Italiana Di Meccanica Teorica Ed Applicata, National Congress*, Naples, Italy, October 1974, Milan, Associazione Italiana Di Meccanica Teorica Ed Applicata, P in Italian.

[3] S. Liao, C. Wu, and D. Ji, "Launch dynamics modeling and analysis on influencing factors for airborne missile," *Journal of Projectiles, Rockets, Missiles and Guidance*, vol. 33, no. 3, pp. 153–156, 2013.

[4] X. Yelun, *Flight Theory in Atmospheric Perturbation*, National Defense Industry Press, 1993.

[5] Z. Hu, *Gust load analysis and alleviation for an elastic aircraft, [M.S. thesis]*, Nanjing University of Aeronautics and Astronautics, 2016.

[6] W. Gao, *The adaptive feed-forward control of gust load for an elastic aircraft, [M.S. thesis]*, Nanjing University of Aeronautics and Astronautics, 2015.

[7] *25-R3 C.Test Standard for Transport Aircrafts*, Civil Aviation Administration of China, 2011.

[8] S. Zhu and B. Etkin, "Model of the wind field in a downburst," *Journal of Aircraft*, vol. 22, no. 7, pp. 595–601, 2012.

[9] B. Etkin, "Turbulent wind and its effect on flight," *Journal of Aircraft*, vol. 18, no. 5, pp. 327–345, 2012.

[10] C. Yangjian, "Calculation of aircraft response to continuous atmospheric turbulence in time domain," *Flight Dynamics*, no. 2, pp. 27–36, 1994.

[11] F. M. Hoblit, *Gust Loads on Aircraft: Concepts and Applications*, AIAA Education, 1988.

[12] T. Shih, "Overset grids: fundamental and practical issues," in *20th AIAA Applied Aerodynamics Conference*, St. Louis, MO, USA, June 2006.

[13] R. Noack and J. Slotnick, "A summary of the 2004 overset symposium on composite grids and solution technology," in *43rd AIAA Aerospace Sciences Meeting and Exhibit*, Reno, Nevada, January 2015.

[14] J. An, M. Yan, W. Zhou, X. Shan, and Z. Yan, "Aerodynamic-guidance-trajectory simulation of tactical missile," in *Guidance, Navigation and Control Conference*, Boston, MA, USA, August 2013.

[15] A. P. London, L. A. Hundley, and L. J. Droppers, "Airborne rocket launch system," US Patent 9,745,063, 2017.

[16] T. Yang, J. Yang, and L. Chai, "Actuator controller design for UAV airborne short range air-to-ground guided missile based on DSP and CPLD," in *2017 2nd International Conference on Applied Mechanics, Electronics and Mechatronics Engineering*, Beijing, China, 2017.

[17] J. K. Foster, T. M. Jakubowski Jr., and R. Binkholder, "Multiple missile and bomb carriage system," US Patent 15/068,304, 2017.

[18] R. Webster, D. G. Hyams, and K. Sreenivas, "Unstructured grid technology applied to axial-flow compressors," in *48th AIAA Aerospace Sciences Meeting Including the New Horizons Forum and Aerospace Exposition*, Orlando, FL, USA, January 2013.

[19] W. Schiehlen, "Multibody system dynamics: roots and perspectives," *Multibody System Dynamics*, vol. 1, no. 2, pp. 149–188, 1997.

[20] N. Yusen, *Research on internal ballistic flow filed characteristics of self-eject launch, [Ph.D. thesis]*, Beijing Institude of Technology, 2016.

[21] H.-S. Park, Y.-S. Park, and J.-H. Kim, "Dynamic analysis of a rail/canister type missile launcher acted by intermittent contact force," *Journal of the Korean Society for Aeronautical & Space Sciences*, vol. 22, no. 1, pp. 1057–1057, 1994.

[22] E. E. Covert, "Conditions for safe separation of external stores," *Journal of Aircraft*, vol. 18, no. 8, pp. 624–630, 2015.

[23] H. Wang, L. Xiang, W. Xiaopeng, and G. Yuheng, "Safety assessment for store separation," *Aerospace Shanghai*, vol. 34, no. 5, pp. 124–129, 2017.

[24] K. Anandhanarayanan, K. Arora, V. Shah, R. Krishnamurthy, and D. Chakraborty, "Separation dynamics of air-to-air missile using a grid-free Euler solver," *Journal of Aircraft*, vol. 50, no. 3, pp. 725–731, 2013.